Peertechz

Life Sciences Group

International Journal of Nanomaterials, Nanotechnology and Nanomedicine

ISSN: 2455-3492 DOI CC By

Mohammad E Khosroshahi[1-3]* and Maral Asemani[1]

[1]Amirkabir University of Technology, Faculty of Biomedical Engineering, Biomaterial Group, Laser and Nanobiophotonics Laboratory, Tehran, Iran
[2]University of Toronto, Department of Mechanical and Industrial Engineering, Toronto, ON M5S 3G8, Canada
[3]MIS-Electronics, Nanobiophotonics and Biomedical R&D Center, Richmond Hill, ON L4B 1B4, Canada

Dates: Received: 03 May, 2017; **Accepted:** 09 June, 2017; **Published:** 10 June, 2017

***Corresponding author:** Mohammad E Khosroshahi, MIS-Electronics, Nanobiophotonics and Biomedical R&D Center, Richmond Hill, ON L4B 1B4, Canada, E-mail: khosrom@mie.utoronto.ca

Keywords: Magnetites; Fluorescine isothiocynate; Fluorescence imaging; Biomarker; MCF 7 cells

https://www.peertechz.com

Research Article

Synthesis, Characterization and Imaging of Fluorescine Isothiocyanate Conjugated Magnetite Nanoparticles in MCF 7 Breast Cancer Cell Lines

Abstract

In this work we describe fabrication, characterization and possible application of FITC (fluorescine isothiocyanate) conjugated magnetite nanoparticles (MNPs) for biomedical applications such as imaging of cancer cells. The MNPs possessed octahedral-like geometry with almost completely dispersed distribution with high saturation magnetization. The final FMNPs (fluorescine isothiocyanate magnetite nanoparticles) absorption band showed 30 nm red shift towards longer wavelength compared to bare MNP and the laser-induced fluorescence was observed at 518 nm. The MTT (3-(4,5-Dimethylthiazol-2-yl)-2,5-Diphenyltetrazolium Bromide) results showed that FITC conjugation diminishes the toxicity MNPs mainly due to the reduction of surface charge. Fluorescence microscopy confirmed the uptake and distribution of FMNPs in MCF 7 (Michigan Cancer Foundation-7) breast cancer cells, which suggests that it can be utilized for applications such as a magnetic fluorescent probe for bioassay.

Introduction

It is well known that biomarkers (or biological markers) are measurable sign of an organism evaluated as an indicator of normal biological processes, pathogenic processes or pharmacological responses to a therapeutic intervention. Some of potential applications of biomarkers include oncology, screening, differential diagnosis, prediction of response to treatment, and monitoring of progression of disease [1]. Equally important is the critical and effective role that nanotechnology, particularly the nanobiomaterials that can play in achieving the above goals. Indeed, the design and development of a reliable and green chemistry process for synthesis of nanomaterials is an important aspect of ongoing nanotechnology research namely biomedical engineering. Cancer nanotechnology has already shown its capability in revolutionizing the current techniques in cancer early diagnosis, imaging, treatment and prevention [2].

Magnetite, Fe_3O_4, is a common magnetic iron oxide that has a cubic inverse spinel structure with oxygen forming an fcc closed packing and Fe cations occupying interstitial tetrahedral sites and octahedral sites. The electrons can hop between Fe^{2+} and Fe^{3+} ions in the octahedral sites at room temperature, rendering magnetite an important class of half-metallic materials. With proper surface coating, these magnetic nanoparticles can be chemically stable, well dispersed with uniform size distribution. When the size of these nanoparticles becomes so small that their dimension can be considered as a single domain, they lack a hysteresis loop and a possess high field irreversibility, high saturation field and extra anisotropy contributions called superparamagnetic iron oxide nanoparticle (SPION) [3,4]. Over the past decades SPIONs with size and morphology dependent physical and chemical properties including biocompatibility, biodegradability, long blood retention time, chemical composition, magnetic behaviour, surface structure, adsorption properties, solubility, low toxicity, and good magnetic response have attracted world-wide research attention [5-7]. These unique materials have been utilized successfully for number of applications including contrast-enhanced imaging [8,9] and drug delivery due to their magnetic nature which can be manipulated by an external magnetic field [10,11]. In magnetically guided nanoparticles (NPs), a constant external magnetic field is used to transport magnetic NPs loaded with drugs to a specific site within the body or to increase the transfection capacity.

There are number of frequently used imaging modalities which can be utilized to visualize targeted cells or molecules including positron emission tomography (PET), single photon emission computed tomography (SPECT), X-ray computed tomography (CT), magnetic resonance imaging (MRI), optical

Citation: Khosroshahi ME, Asemani M (2017) Synthesis, Characterization and Imaging of Fluorescine Isothiocyanate Conjugated Magnetite Nanoparticles in MCF 7 Breast Cancer Cell Lines. Int J Nanomater Nanotechnol Nanomed 3(2): 044-050. DOI: http://doi.org/10.17352/2455-3492.000020

imaging, photoacoustic imaging and ultrasound imaging [12-16]. In clinical detection and therapy, all modalities play a great role with significant contributions, however, each also has its advantages and disadvantages defined by different parameters such as sensitivity, spatial and temporal resolution, invasiveness (e.g., radiation ionization, dose of radioactive material). Despite the limiting factor of optical technique in deep lying cancer screening within the body's organ, it has key advantages including wavelength sensitivity of tissue intrinsic chromophores, low energy radiation and ability to monitor multiple independent optical biomarkers. Generally, optical imaging is performed in the range of ultraviolet-visible-infrared radiation where it can be in the form of radiative as heat and radiative as fluorescence response. When nanoparticles or probing ligands are suitably conjugated by optical or fluorescent agents, they become smart in such a way that they can be used to identify or target specific biological organs [17]. The fluorescence spectroscopy [18,19] and imaging [20,21] have also been widely used in studying cancer diagnosis.

Despite advantages of *in-Vitro* optical imaging of cancers in clinical studies such as rapid imaging, it has been challenging in obtaining high optical quality that distinguishes between healthy and cancer tissues. Recent advances were made to enhance the imaging quality by making target tumor tissue as source of light. Imaging agents play a significant role in labelling target molecules for detection of their population and distributions. As a conventional silanisation reagent, APTS can introduce amine groups onto the surface of the nanoparticle. In this way, one of the three ethoxy groups ($-O-CH_2-$ CH_2- CH_3) initially present in the APTS molecule breaks off from the molecule, which leads to covalent bonding between the APTS groups and the MNPs [22]. At pH <10, protonation of the amines may give a positive surface charge, which accounts for the high stability of these dispersions. The modification results in products with new functional groups on their surface, capable of interacting with an organic medium, and hence allowing the surface properties to change from typically hydrophilic [silanol groups, which can be easily coupled with 3-aminopropyltriethoxysilane (APTS) to hydrophobic (lyophilic) ones. The active amino groups ($-NH_2$) facilitate the further functionalization and can covalently bond with other active groups, such as the carboxyl (−COOH) that can conveniently conjugate with antibodies and other functional groups. Consequently, specific targeting and multifunctionalization can be realized. Additionally, the modified magnetic NPs with amino silane shell are non-toxic, biocompatible and injectable.

FITC is a derivative of fluorescein used in various applications such as flow cytometry and it is the original fluorescein molecule functionalized with an isothiocyanate reactive group (-N=C=S), replacing a hydrogen atom on the bottom ring of the structure, figure 1A combination of different imaging techniques such as optical imaging and imaging agents such as FITC can provide complementary information about the imaged target. FITC allows facile labelling of various structures and has been employed in laser-induced fluorescence detection techniques and flow cytometry of protein labelling [23,24]. In our recent report, it was shown that the emission of FITC intensity is pH-dependent which can be considered as an advantage since tumors or inflamed tissues are relatively acidic, about 6.5, due to hypoxic conditions [25] thus, the fluorescence intensity can be used as an easy monitoring probe. Also, it was recently reported by our group that SPION-based plasmonic nanodendrimers can have the potential capability to be utilized for thermal and bioimaging applications [26,27]. In this research, the results of synthesized SPIONs functionalized by fluorescine isothiocynate (FITC) used as biomarker for fluorescence imaging of L929 and MCF 7 cancer cell lines are described.

Materials and Methods

Materials

All analytic reagents including ferric chloride hexahydrate ($FeCl_3.6H_2O$, 99%), ferrous chloride tetrahydrate ($FeCl_2$. $4H_2O$, 99%) and hydrochloric acid (HCl 37%), ammonia aqueous (25 wt %), sodium hydroxide of (NaOH > 99%), 3-amino-propyl-triethoxy-silane [$3NH_2$ $(CH_2)3Si$ (OC_2H_5), APTS], Milli-Q water (18.2- MΩ.cm) were purchased from Merck and used without further purification and fluorescein isothiocyanate (FITC) was purchased from Aldrich Chemical Co. Dulbecco's Modified Eagle Medium (DMEM) culture medium was purchased from Sigma-Aldrich.

Synthesis of Magnetite nanoparticles MNPs

1.28 M ferric chloride hexahydrate, 0.64 M ferrous hetrahydrate and 0.4 M hydrochloric acid were prepared as a source of iron by dissolving the respective chemicals in 18.2 M milli-Q water and deoxygenated by bubbling N_2 gas for 1 h prior to the use under vigorous stirring. In the same way, an optimized value of 1.5 M NaOH were prepared as the alkali sources [7,28,29]. Aqueous dispersion of magnetic nanoparticles was prepared by alkalinizing an aqueous mixture of ferric and ferrous salts with NaOH at room temperature. 25 mL of iron source was added drop-wise into 250 mL of alkali source under vigorous magnetic stirring at 1500 rpm for 30 min at ambient temperature. The molar ratio of Fe^{2+}: Fe^{3+} = 1:2 and complete precipitation of Fe_3O_4 between 7.5-14 pH was maintained under a non-oxidizing environment, since this would critically affect the physical and chemical properties of the nanosized magnetic particles. The precipitated powder was isolated by applying an external magnetic field, and the supernatant was removed from the precipitate by decantation. The powder was washed and the solution was decanted twice after centrifugation at 5000 rpm for 15 min. Then 0.01M HCl was added to neutralize the anionic charge on the particle surface.

Amino-Silane Functionalization of SPIONs

Typically, 25 ml of magnetite colloid ethanol solution was prepared, and then diluted to 150 ml by ethanol and 1 ml H_2O. The solution was treated by ultrasonic wave for 30 minutes and followed by adding 35µl 3-aminopropyltriethoxysilane [$3NH_2(CH_2)3Si(OC_2H_5)$, APT S] to it and stirred for 7 h. The solution was finally washed five times with ethanol and then dried into powder at room temperature under vacuum.

Citation: Khosroshahi ME, Asemani M (2017) Synthesis, Characterization and Imaging of Fluorescine Isothiocyanate Conjugated Magnetite Nanoparticles in MCF 7 Breast Cancer Cell Lines. Int J Nanomater Nanotechnol Nanomed 3(2): 044-050. DOI: http://doi.org/10.17352/2455-3492.000020

FITC conjugation of APTS-SPONs

This was obtained between isothiocyanate functional group in FITC structure which has high tendency to react with amine groups on Fe_3O_4 nanoparticles as shown in below:

$$R^1N = C = S + R^2NH_2 \rightarrow R^1NH - \overset{\overset{S}{\|}}{C} - NHR^2$$

For conjugation, 1 ml of 1mg/1 ml of FITC molecules in Dimethyl sulfoxide (CH3)2SO, DMSO solution was added to 20 ml of 0.0128 M of APTS functionalized iron oxide nanoparticles in ethanol. The solution was placed on the shaker at low temperature for 4 h in dark room. The FITC conjugated MNPs were then magnetically separated from ethanol. To remove the unreacted FITC molecules, the MNPs were washed three times by ethanol and distilled water then dispersed in 20 ml of deionized water. The final product was centrifuged and kept in dark container figure 1.

Culture of cell lines

MCF-7 cell lines of (human breast cancer cells) were obtained from National Cell Bank of Iran.

Cells were grown in - Dulbecco's Modified Eagle Medium (DMEM) culture medium at 37 °C under 5% CO_2 in a humidified incubator. The cells were harvested, counted and transferred to 96-well plates (15,000 cells per a well) and incubated for 24 h prior to the addition of nanoparticles. The FMNPs were processed and used in various concentrations, and the treated cells were then incubated for 24 h. 5 mg of MTT the water soluble tetrazolium salt dissolved in 1 mL of phosphate-buffered saline (PBS), and 25 µL of the MTT solution was added to each of the 96 wells. The plates were wrapped in an aluminum foil and incubated at 37 °C for 4 h. The solution in each well, containing media, unbound MTT and dead cells, was removed by suction, and 200 µL of DMSO was added to each well. The plates were then shaken, and the optical density was measured using a microplate reader (Stat tax 2100, USA) at 575 nm. . The MCF-7 cells were then trypsinized, rinsed with DMEM and washed twice with PBS to remove the excess nanoparticles which did not react with cells. The images of cancer cell lines were acquired by an optical and fluorescence microscope using 400× magnification.

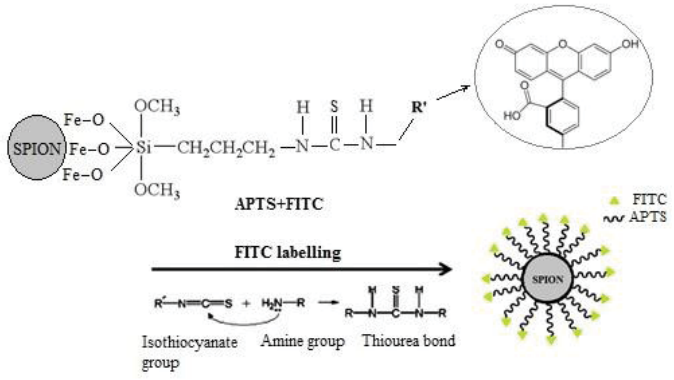

Figure 1: Schematic illustration of synthesis process of conjugating magnetite nanoparticle with FITC.

Characterization

The average size of MNPs was estimated using a transmission electron microscope (Model CM120, PHILIPS). Fourier transformation-IR (FT-IR) spectra of samples were obtained using a FTIR spectrophotometer (NEXUS 670, Nicolet). X-ray diffraction (Cu Kα (λ = 1.5406°A, 40 kV,40 mA, FK60-40) was used to determine the crystalline phase of NPs , the extent of FITC conjugation was measured in a UV visible spectrophotometer (Sunnyvale, CA). Magnetization measurements were carried at 300K in a magnetic field up to 8.5 k Oe with a vibrating sample magnetometer (VSM-PAR 155). Zeta potential of MNP and FMNP along with hydrodynamic diameter of FMNP were determined through zetasizer (Malvern, Nano ZS). The evaluation of fluorescence emission of FMNPs nanoparticles was performed using a tunable ion argon laser Melles Griot-35MAP431 with wavelengths range between (454-514) nm. The fluorescence signals were detected by a 600 µm core diameter optical connected to spectrometer (UV-vis USB 4000, Ocean Optics). Before the measurements, the samples were dried at 15 °C in a vacuum for 6 h. Fluorescence microscopy (Zeiss Axioshop-Germany) was used to study the cells fluorescence).

Results and discussion

As shown in figure 2A, the mean Fe_3O_4 particle size examined by TEM imaging are almost dispersed and figure 2Bshows the APTS functionalized MNPs. It is notable that, the particles have an octahedral-like geometry (Figure 2B). The histogram size distribution covers sizes between (8-20) nm with about 25% count on <12> nm diameter. The influence of the chemical potential on the shape evolution of crystals has been elucidated by Jin et al. [30]. In the case of crystal growth, it would be beneficial to have a higher chemical potential, which is mainly determined by the NaOH concentration. Octahedral Fe_3O_4 with high quality and crystallinity could be obtained in concentrated solution, because higher OH- ion concentration and higher chemical potential in the solution favor the growth of octahedral structures over other possible iron-oxide crystal forms. Crystalline structure of magnetite nanoparticles were analyzed by XRD (Figure 2C). The results confirmed the formation of highly purified magnetite phase of iron oxide with diffraction peaks at (220), (311), (400), (422), (511), (440), which are the characteristic peaks of the Fe_3O_4 inverse spinel structure (JCPDS file No. 19-0629) without any interference with other phases of Fe_xO_y. Since lower pH slows down the oxidation reaction, thus in co-precipitation reaction iron salt solution should be kept at lower pH and temperature prior to precipitation by alkaline media [31]. In this study, the initial pH and temperature of salt solution were adjusted to 1.7 and 25 °C respectively to obtain a pure magnetite phase. The inter-planar space (d-value) of synthesized nanoparticles can be calculated using Bragg equation for the reflection peaks. This can be used to distinguish between γ-Fe_2O_3 and Fe_3O_4 crystallographic structure. Broadening of the dominant intense peak in XRD graph (311) confirms the small size of the resultant particles. The crystalline size of MNPs synthesized at 25°C was calculated as 18 nm using Debay-Sherrer's equation [32].

Citation: Khosroshahi ME, Asemani M (2017) Synthesis, Characterization and Imaging of Fluorescine Isothiocyanate Conjugated Magnetite Nanoparticles in MCF 7 Breast Cancer Cell Lines. Int J Nanomater Nanotechnol Nanomed 3(2): 044-050. DOI: http://doi.org/10.17352/2455-3492.000020

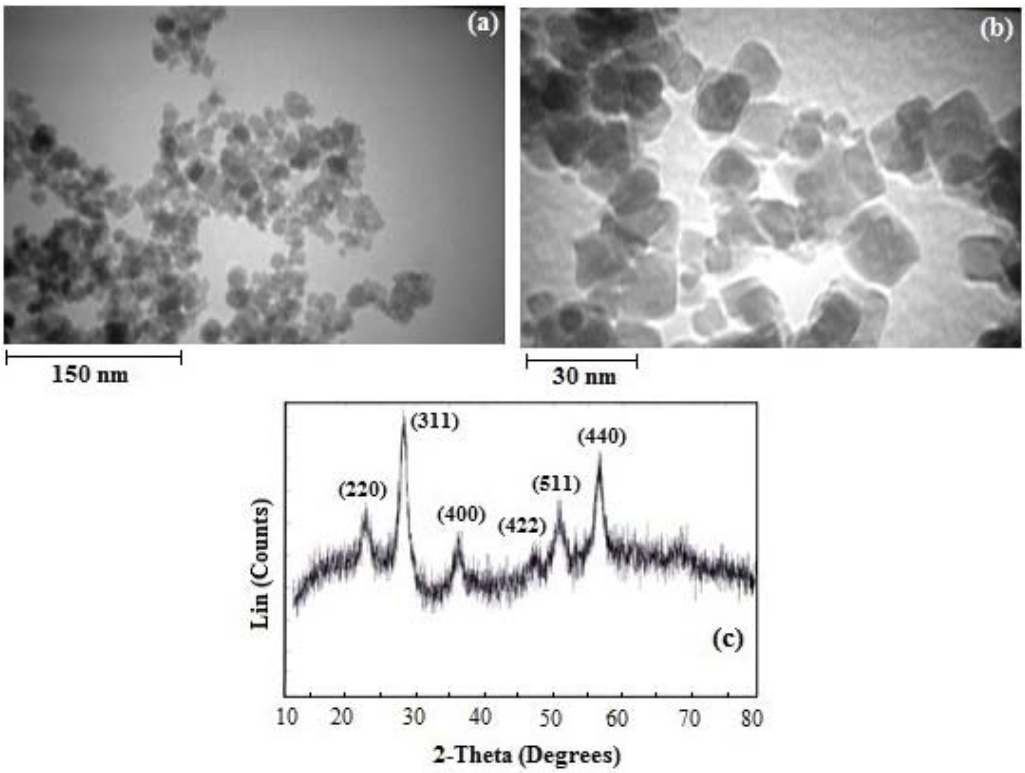

Figure 2: (a) TEM images of (a) MNPs, (b) after functionalization by APTS and (c) X-ray diffraction pattern (XRD) of MNPs.

$$D=\frac{K\lambda}{\beta\cos\theta} \quad (1)$$

In this equation, D, λ and β represent the mean diameter of particles, the wavelength of incident X-ray, and the full width at half height (FWHM) respectively and constant K is equal to 0.9.

To confirm the chemical bonding between APTS molecules and iron oxide nanoparticles and also between FITC molecules and amine functional group at MNP surface, FTIR spectroscopy was performed. Number of important determining factors for adsorption of aqueous solution ions on the surface of MNPs are high surface to volume atoms ratio, high nanoparticle surface energy and number of bonds at the surface. In a neutral solution containing dispersed MNPs, free Fe and O atoms at the surface adsorb H^+ and OH^+ which explains the high density of functional group (-OH).

The FTIR spectra of MNPs are shown in figure 3 where the presence of magnetite, Fe-O, is evident at around 444 cm^{-1}, 591 cm^{-1} and 1420 cm^{-1} and 1560 cm^{-1} and 3413 cm^{-1} show -OH bonds. The peaks related to Fe-O bonds at amine group functionalized MNP surface are shifted to higher wavenumbers of 477 cm^{-1} and 620 cm^{-1} respectively compared to pure Fe_3O_4 NPs, which confirms Fe-O-Si bond formation. Also, the Fe-O-H groups at Fe_3O_4 surface are replaced by Fe-O-Si(O-)$_2$-R.

In figure 3B, the 1118 cm^{-1} and 1403 cm^{-1} represent the stretching vibration of Si-O and CH_2 bands respectively and those near 1623 cm^{-1} and 3414 cm^{-1} the NH_2. Figure 3C,D represents the results of MNPs conjugated by FITC and FITC respectively, where the bonds at 1109 cm^{-1}, 1625 cm^{-1}, 2029 cm^{-1} and 3413 cm^{-1} correspond respectively to C-N stretched-vibrational, rotational-vibrational of amine, vibrational groups of CO present in FITC molecule structure and the vibrational group of –OH present in FITC molecule structure. The vibrational group of isothiocyanate (-NCS) is shown at 2100 cm^{-1} in figure 1D. It worth to note that this band does not exist in figure 1C i.e., FITC conjugated magnetites due to fact that during the reaction between isothiocyanate group and amine, the functional group of (-NCS) in the FITC molecule structure is converted to thiourea (NH-CS-NH-) group.

Saturation magnetization (Ms), residual magnetization (Mr) and coercivity (Hc), are among the main magnetic parameters. Figure 3E shows the room-temperature magnetization curve of the bare MNPs where the hysteresis loop exhibits a reversible behaviour implying the magnetization curve has zero remanence and Hc. The Ms value was measured 50 emu g^{-1} at 6000 Oe and when the external magnetic field was removed, the particles redispersed rapidly. This relatively fast magnetic response can be an advantage in many applications. In the case of Fe_3O_4 conjugated FITC, figure 3F the Ms value decreased to about 40 $emug^{-1}$ indicating that FITC coating can lead to the formation of a nonmagnetic layer on top of the magnetic core which can consequently decrease the magnetization of the nanoparticles [19]. It is reported in the literature that Ms of iron-oxide nanoparticles increases with increase in particle size [5,7,32]. In addition, it may also be due to different chemical compositions on the surface like oxidation of Fe_3O_4 to Fe_2O_3, surface effect such as nonlinearity of spins of magnetically

Citation: Khosroshahi ME, Asemani M (2017) Synthesis, Characterization and Imaging of Fluorescine Isothiocyanate Conjugated Magnetite Nanoparticles in MCF 7 Breast Cancer Cell Lines. Int J Nanomater Nanotechnol Nanomed 3(2): 044-050. DOI: http://doi.org/10.17352/2455-3492.000020

inactive layer with the magnetic field. Also, the discrepancy could be explained by the variation of synthesizing methods which can produce particles of different size [33]. Pinning is one of the main sources of the H_c. Grain size dependence of H_c and permeability (GSDCP) theory [34] predicts:

$$H_c = P_1 \frac{\sqrt{AK}}{M_s D_g} \mu 1/D_g \quad (2)$$

where A denotes the exchange constant, K is a magneto crystalline anisotropy constant, P_1 and P_2 are dimensionless factors. Therefore, reducing the grain size, D_g, creates more pining sites and increases H_c. For ultrafine particles, the modified form of theory predicts:

$$H_c = P_2 \frac{K^4 D_g^6}{M_s A} \mu D_g^6 \quad (3)$$

The difference between equations (2) and (3) is defined by ferromagnetic exchange length as:

$$L_{ex} = \sqrt{A/K} \quad (4)$$

Using the following parameters for magnetite (K=1.35×10^4 J/m^3, A=10^{-11} J/m), the exchange length can be estimated as L_{ex} = 27 nm.

The results of absorption spectroscopy for FITC, MNPs and MNPs conjugated FITC are shown in figure 4A. Clearly, there are two distinct broad bands for FITC between 220-250 nm and 400-500 nm with maximum peaks centered at 220 and 450 nm respectively, which mainly correspond to –NH bond. The iron oxide nanoparticles showed their typical characteristic absorption continuum in the range of 320-370 nm [35]. However, when MNPs were conjugated with FITC, the 400-500 nm band was shifted towards a longer bandwidth of 450-520 nm with maximum peak at 480 nm with significant reduced amplitude showing about 30 nm red shift which corresponds to thiourea bond in FMNPs. Figure 4B illustrates the result of laser-induced fluorescence of FMNPs excited at 488 nm with a typical emission peak at 518 nm.

The results of MTT assay after 24 h at different concentrations from 10 to 500 µg/mL are shown in figure 5. As it is seen, as the concentration increases, the cellular compatibility of samples is reduced. At the lowest concentration

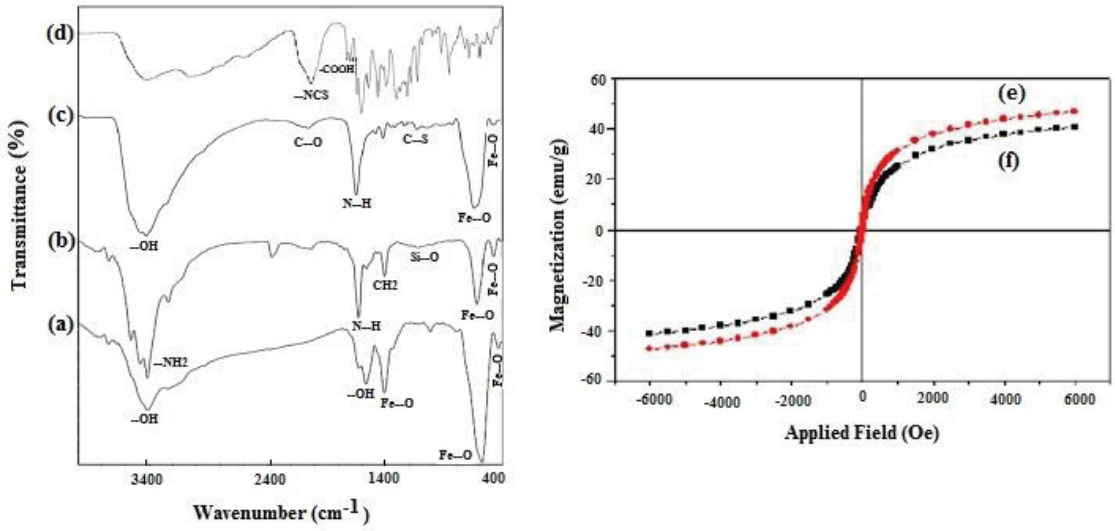

Figure 3: FTIR spectra of (a) MNPs, (b) APTS functionalized MNPs, (c) APTS functionalized MNPs labelled by FITC, (d) FITC molecules only, (e) vibrating sample manometry (VSM) of MNPs and (f) FMNP.

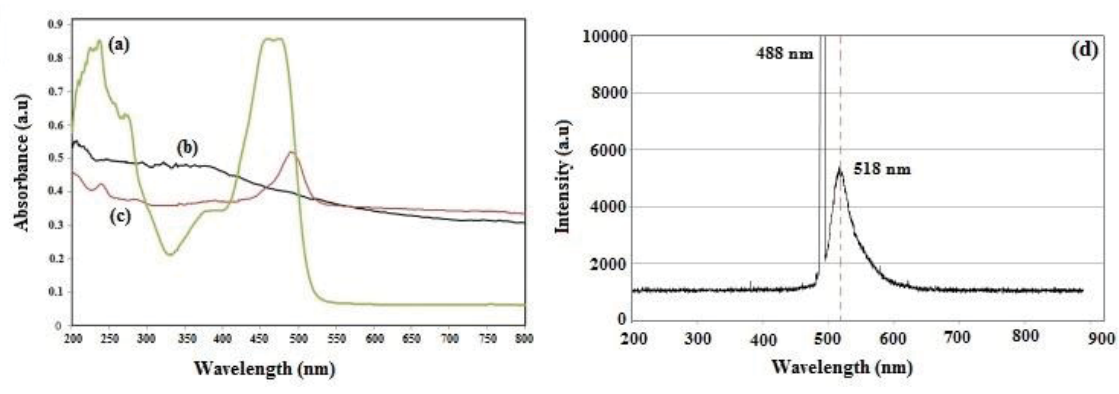

Figure 4: UV-Vis absorption spectroscopy of (a) FITC, (b) MNPs and (c) FMNP and (d) Laser-induced fluorescence spectra of FMNP.

Citation: Khosroshahi ME, Asemani M (2017) Synthesis, Characterization and Imaging of Fluorescine Isothiocyanate Conjugated Magnetite Nanoparticles in MCF 7 Breast Cancer Cell Lines. Int J Nanomater Nanotechnol Nanomed 3(2): 044-050. DOI: http://doi.org/10.17352/2455-3492.000020

value of 10 µg/mL, the cell viability was about 63% and 70% and as the concentration further increased to 500 µg/mL, the viability was reduced to 23% and 60% for MNPs and FMNPs respectively. It is worth note that up to 100 µg/mL, the viability remained almost constant for FMNPs. Thus, the conjugation of MNPs with FITC significantly reduced the toxicity mainly due to the reduction of surface charge. Therefore, with FITC on the surface, the cytotoxicity effect due to direct contact of cell membrane with MNP surface can be reduced.

Optical microscope images of FMNP incubated MCF7 after 24 h is shown in figure 6. The morphology of cells at low concentrations of FMNP is very similar to the control sample. As gradually the concentration of FMNPs increase in samples (Figure 5 A-C), the cells tend to change into more round shape due to accumulation of nanoparticles on the cell surface and probably internalization of nanoparticles. The fluorescence intensity is clearly enhanced with increasing the concentration of FMNPs (Figure 5 D,E). The distribution of dispersed FMNPs inside a static colloidal medium (e.g., petri dish with cell culture medium) can be considered as Brownian motion using Lorentzian distribution as normally is considered in soft matter physics. Therefore, one may assume

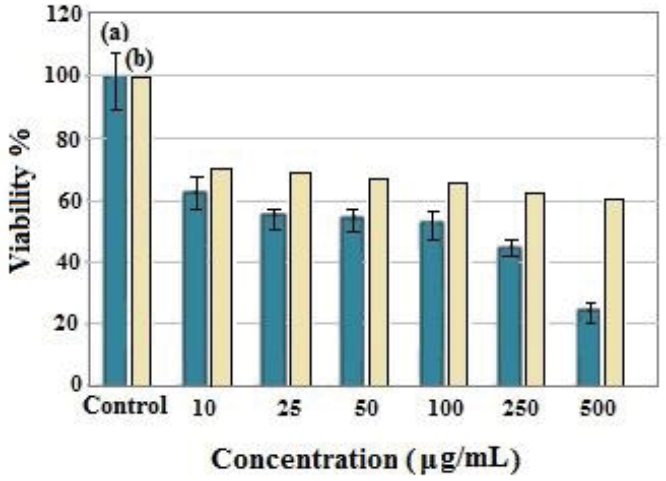

Figure 5: Variation of cell viability at various exposure dosages (10–500 µg/mL) of (a) MNPs (b) FMNP samples incubated MCF-7 cell lines for 24 h.

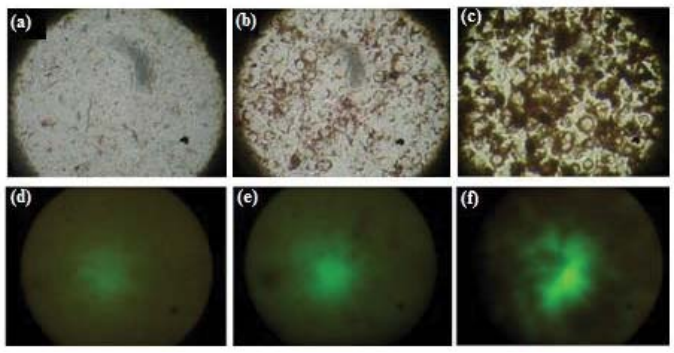

Figure 6: Bright- field microscopy of MCF 7 cell images with 400×magnification after incubating with FMNPs at different exposure dosage for 24 h, (a) 10 µg/ml, (b) 250 µg/ml, (c) 500 µg/ml. Comparison of fluorescence microscope images of FMNPs after 24 h, (d)10 µg/ml, (e) 250 µg/ml,(f) 500 µg/ml.

that $\Psi(r')=d3r'ND(r')$ where $\Psi(r')$ is the probability of finding a NP at a distance, r′ in a volume d3r′ and ND (r′) is a density distribution of NPs, a function which decays according to the spatially damped radial function [36]. Thus, two possible sources could be sought, firstly the diffusion or mobility due to stronger Brownian motion within the dish which takes place radially and secondly the extra eddy micro currents acting as non-uniform source of distribution when the NPs were added in the experiment. In either case, the fact remains that the images prove their conceptual applications as molecular probes which can provide a better detection and hence understanding of cellular mechanisms.

Conclusion

FITC conjugated iron oxide nanoparticles were synthesized and characterized for biomedical imaging applications. The MNPs exhibited no hysteresis loop and relatively large saturation magnetization with zero remanence and coercivity. The 450-520 nm signal of FMNPs suggests that such structure can be utilized as biomarkers in cellular imaging. This was confirmed by an *in-vitro* assay using MCF 7 cancer cell lines where higher concentration of FMNPs exhibited stronger fluorescence signal with relatively uniform cellular distribution.

Acknowledgment

This research was supported by AUT under faculty grant program. The authors are also thankful to Dr M. Tajabadi from Faculty of Biomedical Engineering, AUT for her help.

References

1. Henry N, Hayes D (2012) Cancer biomarkers. Mol Oncol 6: 140-146. Link: https://goo.gl/41kPxe

2. Grobmyer S, Iwakuma N, Sharma P, Moudgil BM (2010) What is cancer nanotechnology. Methods Mol Biol. 624: 1-9. Link: https://goo.gl/P4WmnM

3. Pankhurst Q, Connolly J, Jones S, Dobson J (2003) Applications of magnetic nanoparticles in Biomedicine. J Phys D: Appl Phys 36: 167-181. Link: https://goo.gl/ztfR3w

4. Gupta A, Gupta M (2005) Synthesis and surface engineering of iron-oxide nanoparticles for biomedical applications. Biomaterials 26: 3995-4021. Link: https://goo.gl/3JAHfg

5. Jiang Q, Lang X (2007) Size dependence of structures and properties of materials. Open Nanosci J 1: 32-59. Link: https://goo.gl/SgGK2n

6. Pisanic I, Blackwell J, Shubayev V, Fiñones R, Jin S (2007) Nanotoxicity of iron oxide nanoparticle internalization in growing neurons. Biomaterials 28: 2572-2581. Link: https://goo.gl/fNReAs

7. Khosroshahi M E, Ghazanfari L (2010) Preparation and characterization of silica-coated iron-oxide bionanoparticles under N_2 gas. Physica E 42: 1824-1829. Link: https://goo.gl/A8grym

8. Corot C, Robert P, Idee J, Port M (2006) Recent advances in iron oxide nanocrystal technology For medical imaging. Adv Drug Del 58:1471-1504. Link: https://goo.gl/MST7Rn

9. Yang R, Fu C, Fang J (2007) Hyaluronan-modified superparamagnrtic iron oxide nanoparticles for biomedical breast cancer imaging and photothermal therapy. Int J Nanomed 17: 197-206. Link: https://goo.gl/j9RvNl

10. Unterweger H,Tietze R, Janko C, Zaloga J (2014) Development and

Citation: Khosroshahi ME, Asemani M (2017) Synthesis, Characterization and Imaging of Fluorescine Isothiocyanate Conjugated Magnetite Nanoparticles in MCF 7 Breast Cancer Cell Lines. Int J Nanomater Nanotechnol Nanomed 3(2): 044-050. DOI: http://doi.org/10.17352/2455-3492.000020

characterization of magnetic iron oxide nanoparticles with a cisplatin-bearing polymer coating for targeted drug delivery. Int J Nanomed 4: 3659-3676. Link: https://goo.gl/OecFYK

11. Estelrich J, Escribano E, Queralt J (2015) Busquets M, Iron oxide nanoparticles for magnetically-guided and magnetically-responsive drug delivery. Mol Sci 16: 8070-8101. Link: https://goo.gl/3fL95l

12. Huang Y, He Sh, Cao W, Liang X (2012) Biomedical nanomaterials for imaging-guided cancertherapy. Nanoscale 4: 6135-6149. Link: https://goo.gl/1AufK3

13. Cherry S (2009) Multimodality imaging: Beyond PET/CT and SPECT/CT. Semin Nuclear Med 39: 348-353. Link: https://goo.gl/HUvQdQ

14. Zhou Z, Zhang Ch, Qian Q (2013) Folic acid conjugated silica capped gold nanoclusters for targeted fluorescence/X-ray computed tomography imaging. J Nanobiotech 11: 1-13. Link: https://goo.gl/E8D1gy

15. Thomas R, Park I, Yong J (2013) Magnetic iron oxide nanoparticles for multimodal imaging and therapy of cancer. 14: 15910-15930. Link: https://goo.gl/N8DWyd

16. Khosroshahi M E, Mandelis A, Lashkari B (2015) Frequency-domain photothermoacoustic and ultrasonic imaging of blood and opto-thermal effects of plasmonic nanoparticle concentrations. J Biomed Opt 20: 076009. Link: https://goo.gl/lnDJmP

17. Hoffman R (2002) *In-vivo* imaging of metastatic cancer with fluorescent proteins, Cell death and Differentiation. 9: 786-789. Link: https://goo.gl/YKxkn7

18. Khosroshahi M E, Rahmani M (2012) Detection and evaluation of normal and malignant cells using laser-induced fluorescence spectroscopy. J Fluoresc 22: 281-288. Link: https://goo.gl/tYiLNe

19. Ra H, Emilio González G, Uddin M, King L (2015) Detection of non-melanoma skin cancer by *in vivo* fluorescence imaging with fluorocoxib A. Neoplasia 17: 201-207. Link: https://goo.gl/aSilve

20. Ntziachristos V, Bremer Ch, R (2003) Weissleder, Fluorescence imaging with near infrared light:new technological advances that enable *in-vivo* molecular imaging. Eur Radiol 13: 195-208. Link: https://goo.gl/Q117Ls

21. Zhang J, Xuehong Y, Lakowicz J (2011) Target molecule imaging on tissue specimens by fluorescent metal nanoprobes. J Biomed Opt 16: 116004. Link: https://goo.gl/tnBS5O

22. Khosroshahi ME, Ghazanfari L (2011) Amino surface modification of Fe_3O_4/SiO_2 nanoparticles for bioengineering applications. Surf Eng 27: 573-580. Link: https://goo.gl/E26UzJ

23. Magali J, Hernandez A, Maurras A, Puget K, Amblard M, et al. (2009) N-terminus FITC labelling of peptides on solid support:the truth behind the spacer. Tetrahedron Lett 50: 260-263. Link: https://goo.gl/V1N4dh

24. Rezvani Alanagh H, Khosroshahi ME, Tajabadi M, Keshvari H (2014) The effect of pH and magnetic field on the fluorescence spectra of fluorescein isothiocyanate conjugated SPION- dendrimer nanocomposites. J Supercond Nov Magn 27: 2337-2345. Link: https://goo.gl/mif8iv

25. Bae Y, Nishiyama N, Fukushima S, Koyama H (2005) Preparation and biological characterization of polymeric micelle drug carriers with intercellular pH-triggered drug release property. Bioconjugate Chem 16: 122-130. Link: https://goo.gl/YUqP0V

26. Tajabadi M, Khosroshahi ME, Bonakdar Sh (2015) Imaging and therapeutic applications of optical and thermal response of SPION-based third generation plasmonic nanodendrimers. Optics and Photon J 5: 212-226. Link: https://goo.gl/u6kwr1

27. Khosroshahi ME, Tajabadi M (2016) Characterization and cellular fluorescence microscopy of superparamagnetic nanoparticles functionalized with third generation nanomolecular dendrimers: in-vitro cytotoxicity and uptake study. J Nanomat Mol Nanotech 5: 1-11. Link: https://goo.gl/e6jB9i

28. Kim D, Zhang Y, Voit W (2001) Synthesis and characterization of surfactant-coated superparamagnetic monodispersed iron oxide nanoparticles. J Mag Mag Mat 225: 30-36. Link: https://goo.gl/J1htJz

29. Liu Z, Liu Y, Yao K (2002) Synthesis and magnetic properties of Fe_3O_4 nanoparticles. J Mat Syn Proc 10: 83-87. Link: https://goo.gl/LcQiML

30. Jin M, Shu H, Pei L, Lu W (2013) Role of Chemical Potential in Tuning Equilibrium Crystal Shape and Electronic Properties of Wurtzite GaAs Nanowires, J Phys Chem C 117: 23349-23356. Link: https://goo.gl/u4smqU

31. Tajabadi M, Khosroshahi ME, Bonakdar Sh (2013) An efficient method SPION synthesiscoated with third generation PAMAM dendrimer, Colloids and Surf. A: Physicochem. Eng Aspects 431: 18-26. Link: https://goo.gl/lg8Hrg

32. Faiyas A, Vinod E, Joseph J, Ganesan R, Pandey R (2010) Dependence of pH and surfactant effect in the synthesis of magnetite (Fe_3O_4) nanoparticles and its properties. J Mag Mag Mat 322: 400–404. Link: https://goo.gl/GbWPof

33. Mohapatra S, Pramanik N, Mukherjee S, Ghosh S, Pramanik P (2007) A simple synthesis of amine-derivatized superparamagnetic iron oxide nanoparticles for bioapplications. J Mater Sci 42: 7566-7574. Link: https://goo.gl/A2c8uk

34. Xue D, Chai G, Li X, Fan X (2008) Effects of grain size distribution on coercivity and permeability of ferromagnets. J Magn Magn Mater 320: 1541. Link: https://goo.gl/a6AnJ4

35. Brown K, Walter DG, Natan M (2000) Seeding of colloidal Au nanoparticle solutions. 2. improved control of particle size and shape. J Chem Mater 12: 306-313. Link: https://goo.gl/TVDMrD

36. Baba-Ahmed L, Benmouna M, Grimson M (1987) Elastic scattering from charged colloidal dispersions. Phys Chem Liquids Int J 16: 235-240. Link: https://goo.gl/8MoYKs

Citation: Khosroshahi ME, Asemani M (2017) Synthesis, Characterization and Imaging of Fluorescine Isothiocyanate Conjugated Magnetite Nanoparticles in MCF 7 Breast Cancer Cell Lines. Int J Nanomater Nanotechnol Nanomed 3(2): 044-050. DOI: http://doi.org/10.17352/2455-3492.000020